Clim Dyn (2017) 48:2135–2151
DOI 10.1007/s00382-016-3196-2

Asymmetry of the winter extra-tropical teleconnections in the Northern Hemisphere associated with two types of ENSO

Juan Feng[1] · **Wen Chen**[1] · **Yanjie Li**[2]

Received: 10 October 2015 / Accepted: 20 May 2016 / Published online: 28 May 2016

Abstract Asymmetric atmospheric responses to ENSO are revisited after dividing it into two types: eastern-Pacific (EP) and central-Pacific (CP) ENSO. The EP ENSO triggers two obvious asymmetric atmospheric teleconnections: One is the Pacific–North American-like teleconnection. Its asymmetry is characterized by weaker amplitudes during the EP La Niña than EP El Niño, which is caused by a much weaker EP La Niña tropical forcing and the resultant weaker extra-tropical vorticity forcing. The other is the Atlantic–Eurasian teleconnection with negative height anomalies in the subtropical Atlantic and Eurasia and positive anomalies in the high-latitude Atlantic and northeast Asia, which appears during the EP La Niña but not during the EP El Niño. The background state plays a vital role in this asymmetry. The EP La Niña-type basic state is more conducive to propagation of the wave rays into the Atlantic–Eurasian region compared to EP El Niño situation. In contrast, the CP ENSO yields an Arctic Oscillation-like teleconnection, presenting an appreciable asymmetry in the subtropical amplitudes that are stronger during the CP El Niño than during the CP La Niña. In this case, the distinct effects of the different background state on the equatorward wave rays are responsible for this asymmetry. Under the CP El Niño-type background state, the equatorward wave rays tend to be reflected at the latitudes where the zonal wind equals zero (U = 0), and then successfully captured by the subtropical westerly jet. However, under the CP La Niña-type background state, the equatorward wave rays disappear at U = 0 latitudes.

Keywords Eastern-Pacific ENSO · Central-Pacific ENSO · Asymmetry · Teleconnection

1 Introduction

El Niño-Southern Oscillation (ENSO) is one of the most important predictors for the global climate anomalies (Coelho and Goddard 2009; Larkin and Harrison 2005; Wu et al. 2003). Its impact is not only confined to the tropics but extends to extra-tropics through teleconnections (Gershunov and Barnett 1998; Horel and Wallace 1981; Wang et al. 2008b). When an El Niño happens, generally, increased rainfall and intensified convection in the tropical central and eastern Pacific is driven by the positive sea surface temperature (SST) anomalies and the opposite condition in the tropical western Pacific is induced by the negative SST anomalies (e.g., Trenberth and Caron 2000). The associated anomalous diabatic forcing in turn triggers atmospheric circulation anomalies propagating from tropics to the mid-high latitudes. For example, the Pacific–North American (PNA) teleconnection as an extra-tropical response to the ENSO forcing extends the impacts of ENSO to the North Pacific and North America (Simmons et al. 1983; Gershunov and Barnett 1998). A Pacific-east Asian teleconnection (PEAT) induced by the ENSO events exerts substantial impacts on the climate anomalies in East Asia (Wang et al. 2000).

Generally, climate anomalies associated with El Niño are considered to be the inverse of those associated with La Niña. Then linear methods, such as correlation and

✉ Juan Feng
juanfeng@mail.iap.ac.cn

[1] Center for Monsoon System Research, Institute of Atmospheric Physics, Chinese Academy of Sciences, P.O. Box 2718, Beijing 100029, China

[2] LASG, Institute of Atmospheric Physics, Chinese Academy of Sciences, Beijing, China

regression, are usually employed by most of the studies (e.g., Chowdary et al. 2012; Wang et al. 2008a; Wu et al. 2003; among others). Actually, climate responses to ENSO are not simply opposite, but show an apparent nonlinearity between the warm and cold phases (Zhang et al. 2014a, 2015). Even if the El Niño and La Niña have the same amplitude and pattern, the climate responses are still asymmetric even in the tropical regions. This is caused, on the one hand by the zonal asymmetry of the climatological SST in the tropical Pacific, and on the other hand by the threshold (27–28 °C) of the occurrence of convection. With respect to the warmer climatological SST over the tropical western Pacific, small SST deviations are capable of inducing large rainfall anomalies, while for the cooler climatological SST over the tropical eastern Pacific, strong SST anomalies are required to induce the convective anomalies. Due to these features, the location of tropical rainfall anomalies associated with El Niño usually shifts eastward relative to the condition during the La Niña events (Deser and Wallace 1990).

Asymmetric responses of tropical rainfall to the warm and cold ENSO forcing inevitably induce the nonlinearity of extra-tropical teleconnections. Hoerling et al. (1997, 2001) reported that the PNA pattern forced by the tropical SST anomalies presents a strong asymmetry in the spatial pattern. Its activity center exists 35° longitude shift between the warm and cold ENSO, causing different climate anomalies over North America (Hoerling et al. 1997, 2001). Moreover, the atmospheric circulation anomalies over the North Atlantic region display a tripole pattern during a La Niña winter but a dipole pattern during an El Niño winter (Hannachi 2001). Wu and Hsieh (2004) demonstrated that the impact of ENSO on the Euro-Atlantic winter sea level pressure (SLP) is weak if using the linear method. However, when the nonlinearity of the ENSO impact is considered, significant SLP anomalies appear for both the El Niño and La Niña.

More recently, another type of ENSO draws attention with warming (cooling) SST anomalies in the tropical central Pacific, which is referred to as the central-Pacific (CP) ENSO or ENSO Modoki (Ashok et al. 2007; Ashok and Yamagata 2009; Kao and Yu 2009; Kug et al. 2009). It is completely different from the conventional ENSO with warming (cooling) SST anomalies in the tropical eastern Pacific (i.e., eastern-Pacific (EP) ENSO) in both the spatial pattern and climate impacts (Feng et al. 2010, 2011; Weng et al. 2007; Wang and Wang 2014; Yang and Jiang 2014; Yu and Kim 2011; Zhang et al. 2013; among others). For example, Weng et al. (2007, 2009) gave us a general comparison of the impacts of CP and EP El Niño on the Pacific rim regions for the winter and summer seasons. Yuan et al. (2012) suggested that evolutions of the anomalous Philippine Sea anticyclone that bridges El Niño to the East Asian climate display distinct features in the location, intensity and lifetime for the CP and EP ENSO through the linear partial correlation method. Until now, most of the related studies mainly focus on the linear influences of two types of ENSO on the climate anomalies. An increasing number of recent studies start to pay attention to the nonlinear impacts of two types of ENSO on the climate. For example, asymmetry roles of the CP (EP) El Niño and La Niña in Australia and the southeast China rainfall variability were reported in the work of Cai et al. (2010) and Karori et al. (2013), respectively. Frauen et al. (2014) documented the asymmetric responses of the sea level pressure (SLP) and tropical rainfall anomalies to the two types of ENSO through the atmospheric general circulation model.

In addition, if only the linear method is employed to explore the ENSO-induced teleconnections, the signal may not be significant at some areas and thus usually be ignored. For example, the studies about the ENSO-related Eurasian climate anomalies are not as many as North America and the North Atlantic. It is possibly because the Eurasian climate responses to ENSO are weak when only the linear impacts are considered (Wu and Hsieh 2004). Moreover, in some cases the linear methods may be misleading. When the effects of ENSO cold phase do not mirror the opposite effects of warm phase, linear methods may not reflect either situation accurately. Considering these issues, we put our attention to the asymmetric impacts of the EP and CP ENSO on the Northern Hemispheric circulation anomalies and their possible physical mechanisms.

The structure of this study is arranged as follows: Sect. 2 introduces the related data and methods used in this paper. In Sect. 3 we examine the asymmetry of the EP (CP) ENSO-related atmospheric circulation anomalies through the composite methods. The physical reasons that cause this asymmetry between the warm and cold EP (CP) ENSO events are discussed in Sect. 4. Finally, a summary and a discussion are given in Sect. 5.

2 Data and methods

The reanalysis data from the National Centers of Environment Prediction–National Center for Atmospheric Research (NCEP–NCAR) are employed in this study, including geopotential height and wind fields (Kalnay et al. 1996). This dataset has 17 levels in the vertical direction. The horizontal resolution is 2.5° latitudes by 2.5° longitudes. Sea surface temperature data from the Hadley Center Global Sea Ice and Sea Surface Temperature (HadISST) with the 1.0° × 1.0° horizontal resolution is used to analyze the SST anomalies in the EP and CP ENSO (Rayner et al. 2003). The winter is defined from December to February (DJF). The time series from 1950 to 2011 are considered

in this study and the long-term trend is removed before the analysis.

Winter mean Niño3 index and El Niño Modoki index (EMI) are used to identify the EP and CP ENSO, respectively. The Niño3 index is calculated by the averaged SST anomalies over the region (150°W–90 W, 5°S–5°N). The EMI is defined by the area-averaged SST anomalies in the tropical central Pacific (165°E–140°W, 10°S–10°N) minus the area-averaged ones in the tropical western (125°E–145°E, 10°S–20°N) and eastern Pacific (110°W–70°W, 15°S–5°N) (Ashok et al. 2007).

To better classify the two types of ENSO, we required the normalized Niño3 index not only greater (less) than 0.8 (−0.8) but also greater (less) than EMI to define an EP El Niño (La Niña) case. Then, eight EP El Niño cases (1957, 1965, 1972, 1976, 1982, 1986, 1991 and 1997) and seven EP La Niña cases (1955, 1967, 1970, 1975, 1984, 2005 and 2007) are identified. In the same way, a CP El Niño (La Niña) case is defined when the normalized EMI is greater (less) than 0.8 (−0.8) and also greater than Niño3 index. Thus, six CP El Niño (1968, 1977, 1994, 2002, 2004 and 2009) and seven CP La Niña (1973, 1983, 1988, 1998, 1999, 2000 and 2010) cases are chosen through this approach.

It is reported that based on the current indices it is not easy to classify the two types of ENSO, especially for the two types of La Niña (Ren and Jin 2011; Zhang et al. 2014b). Thus, none of the two documents are consensus for the selection of the EP and CP ENSO. There always exist one or two inconsistent samples among the different documents when different separating methods are employed (Ashok et al. 2007; Kao and Yu 2009; Kug et al. 2009; Ren and Jin 2011; Yu and Kim 2013). Nevertheless, similar results of the robust distinct impacts of EP and CP ENSO are obtained among different documents (e.g. Feng et al. 2010; Garfinkel et al. 2013; Kim et al. 2012). Considered the aforementioned issues, it is better to check whether the methods used in this study can successfully divide the two types of ENSO. Figure 1 gives the evolutions of the tropical SST anomalies from the developing phases of ENSO to the decaying phases. For both of EP El Niño and EP La Niña, the maximum SST anomalies are mainly located in the tropical eastern Pacific, exactly to the east of 150°W (Fig. 1a, b). Another remarkable feature is that the SST anomalies show an obvious westward propagation from developing to decaying phases. Thereby, all these features are consistent with a typical EP ENSO event. In contrast, the CP ENSO shows completely different features from EP ENSO in both of the spatial pattern and the evolution of the SST anomalies (Fig. 1c, d). The position of the maximum SST anomalies associated with CP ENSO move westward into the tropical central Pacific, which is exactly located to the west of 150°W (Fig. 1c, d). Meanwhile, the SST

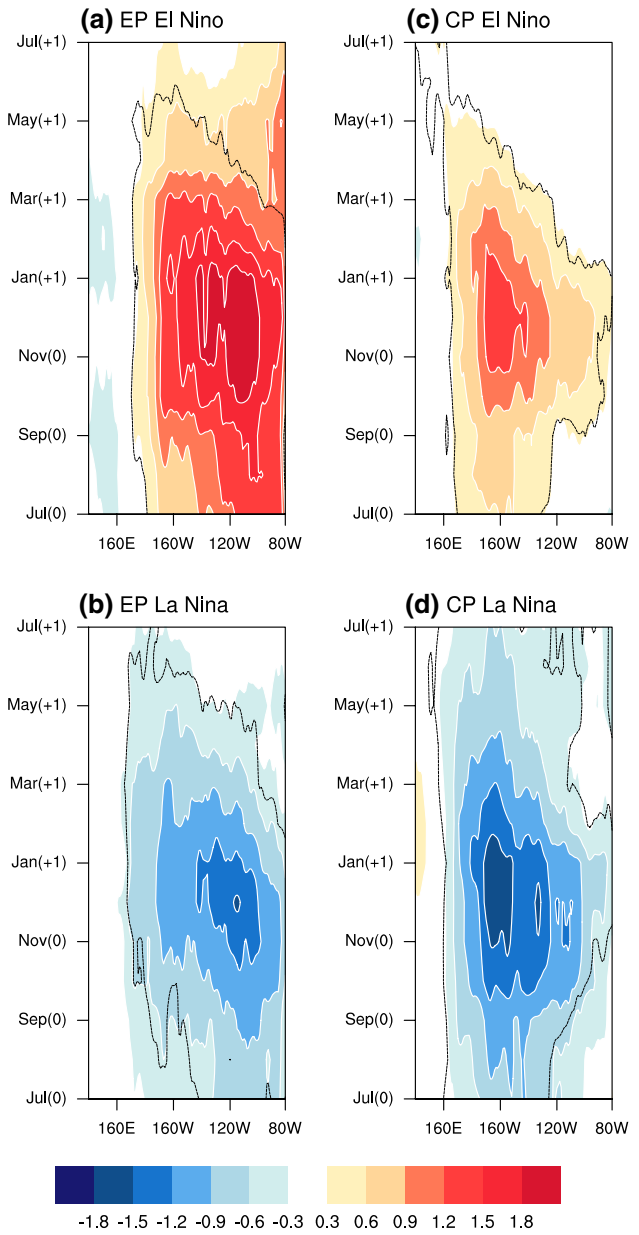

Fig. 1 The time-longitude section of composite SST anomalies (unit: °C) averaged from 5°S to 5°N for **a** EP El Niño, **b** EP La Niña, **c** CP El Niño and **d** CP La Niña events. "0" and "+1" denote the developing and decaying stages of ENSO events, respectively. *Black contours* indicate the 95 % confidence levels based on the two-tailed Student's *t* test

anomalies do not show an obvious propagation feature, but they roughly stay stationary for the whole lifetime instead. Therefore, these differences between the EP and CP ENSO cases in this study are conspicuous and consistent with the distinctions that are defined by the previous studies (Ashok et al. 2007; Kao and Yu 2009; Kug et al. 2009). Thus, not only the two types of El Niño but also La Niña are well separated using our current methods.

The wave activity flux (Takaya and Nakamura 2001) is used to explore the stationary Rossby wave sources and propagation induced by ENSO events. It is a phase-independent flux and is parallel to the local group velocity of a stationary Rossby wave train in the Wentzel–Kramers–Brillouin (WKB) approximation. The horizontal flux is calculated according to the following equation:

$$W = \frac{P}{2|\vec{U}|}\begin{cases} U\left(v'^2 - \psi' v'_x\right) + V\left(-u'v' + \psi' u'_x\right) \\ U\left(-u'v' + \psi' u'_x\right) + V\left(u'^2 + \psi' u'_y\right) \end{cases} \quad (1)$$

where P, $\vec{U} = (U, V)$, ψ' and $\vec{V}' = (u', v')$ denote pressure scaled by 1000 hPa, basic state wind velocity, perturbation geostrophic stream-function and perturbed wind velocity.

3 Asymmetric responses of atmospheric circulation to ENSO

3.1 EP ENSO conditions

Figure 2 shows the composite geopotential height anomalies for the EP El Niño and EP La Niña, respectively. Over the North Pacific and North American regions, the anomalous atmospheric circulation is characterized by a PNA-like teleconnection for the EP El Niño with the negative height anomalies over the North Pacific and positive anomalies over the subtropical Pacific and the North America (Fig. 2a). For the EP La Niña, there exists a similar PNA-like teleconnection with the opposite anomalous centers (Fig. 2b). However, comparing Fig. 2a, b, one can find that the intensity of this PNA-like pattern induced by the EP La Niña is much weaker than that by the EP El Niño, especially for the anomalies over the North Pacific and the North America. Moreover, Hoerling et al. (1997, 2001) presented a significant 35° longitude westward shift of the PNA-like activity centers in the observation and model data for the EP La Niña relative to the EP El Niño. However, after the ENSO is divided into two types, the shift of the PNA-like activity centers between the warm and cold EP ENSO is not as evident as that found by Hoerling et al. (1997, 2001). This westward shift is quite weak in this study, and only the activity center over the North America manifests a westward movement.

Over the Atlantic and Eurasian regions, the atmospheric responses to EP El Niño manifest positive height anomalies over the western part of Europe and negative anomalies over the high-latitude Eurasia, whereas these signals are weak and insignificant (Fig. 2a). In contrast, the geopotential height anomalies during the EP La Niña present much more significant signals, which are characterized by the negative anomalies in the subtropical Atlantic and Eurasian continent and the positive anomalies in the high-latitude North Atlantic and Eurasia (Fig. 2b). These anomalies display alternative (±) sign over the Atlantic–Eurasian region like a stationary Rossby wave. Lin and Derome (2004) suggested that a La Niña forcing usually yields a stronger response over the North Atlantic than an El Niño forcing through a dry atmospheric model, which is in accordance with our results.

To further explore the asymmetric and symmetric impacts of EP ENSO on the atmospheric teleconnections, the composite summation and difference of the geopotential

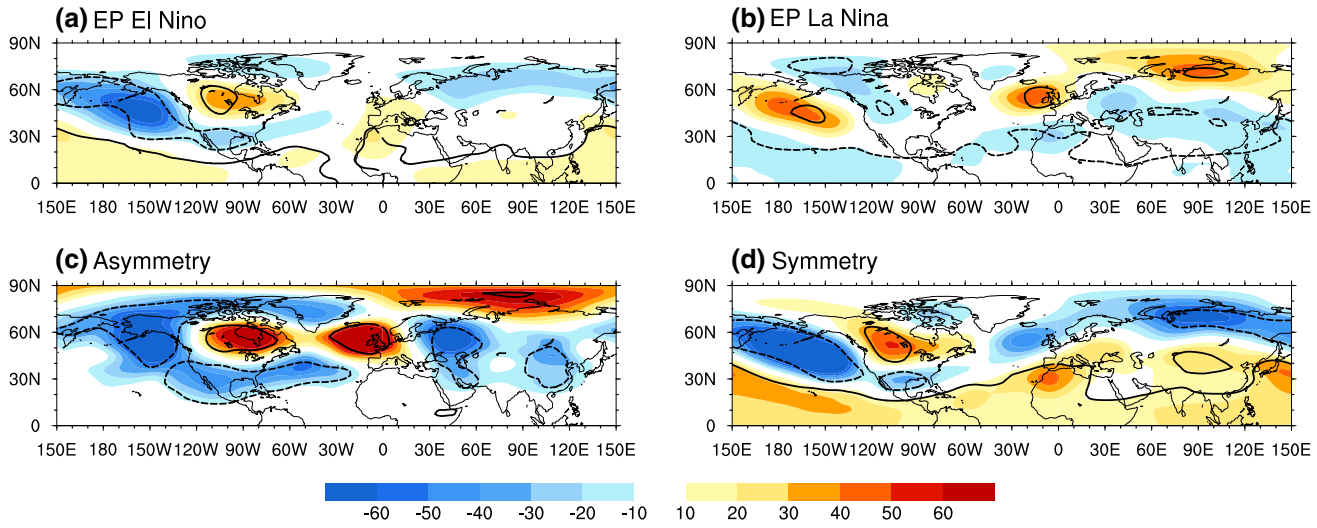

Fig. 2 Composite winter mean (DJF) geopotential height anomalies (*shading*, gpm) at 500 hPa for the **a** EP El Niño (*left column*) and **b** EP La Niña (*right column*), respectively. **c** The asymmetric component is estimated by the summation of **a** and **b**. **d** The symmetric component is estimated by the difference of **a** and **b**. *Contours* denote 95 % confidence levels based on the two-tailed Student's *t* test

height anomalies between the EP El Niño and EP La Niña are shown in Fig. 2c, d, respectively. The summation (difference) estimates the asymmetric (symmetric) components of the EP ENSO responses. The results of the composite summation (Fig. 2c) are multiplied by 2 in order to make a fair comparison with the results of the composite difference (Fig. 2d). The symmetric component of the EP ENSO responses is mainly characterized by the height anomalies over the subtropical Pacific, Aleutian and central parts of North American regions (Fig. 2d), showing a PNA-like pattern. In contrast, the asymmetric component is featured by the robust negative height anomalies over the North Pacific and positive anomalies over the North America (Fig. 2c). This asymmetry is a result of the much stronger amplitudes of the PNA-like teleconnection during the EP El Niño than during the EP La Niña. The weak shift of the PNA-like anomalous center over the North America also makes a contribution to this asymmetric positive anomaly. Meanwhile, another significantly asymmetric component is located over the Atlantic–Eurasian region, with the negative height anomalies over the subtropical Atlantic and Eurasia and positive anomalies over the high-latitude North Atlantic (Fig. 2c). This asymmetry is a reflection of the significant effects of the EP La Niña on the Atlantic–Eurasian regions but not of the EP El Niño.

3.2 CP ENSO conditions

For the CP-ENSO conditions, the atmospheric teleconnections exhibit a distinctive feature compared with those for the EP ENSO due to the different location of warming (cooling) SST anomalies (e.g., Li and Zhou 2012; Yu and Kim 2011; Weng et al. 2009; Zhang et al. 2014a, b). Do the impacts of CP El Niño and CP La Niña on the circulation anomalies have strong asymmetric signals just as the aforementioned conditions for the EP ENSO? To answer this question, the composite geopotential height anomalies for the CP El Niño and CP La Niña are given in Fig. 3. In the case of CP El Niño, the negative geopotential height anomalies extend from the extra-tropical Pacific to the subtropical Atlantic and finally to Eurasia (Fig. 3a). Correspondingly, the high-latitude positive height anomalies stretch from the North Pacific to high-latitude North Atlantic and then reach the northern Eurasia. Thus, the teleconnection associated with CP El Niño displays an Arctic Oscillation (AO)-like annular mode that is completely different from the PNA-like pattern associated with the EP El Niño. This result is in accordance with the previous findings that the atmospheric responses tend to change from the PNA-like to AO-like pattern with the westward movement of the tropical diabatic forcing (Jia et al. 2009). This difference is also revealed by Graf and Zanchettin (2012). They suggested that CP El Niño usually yields an AO-like atmospheric response, while EP El Niño induces a PNA-like teleconnection. During the CP La Niña, a similar AO-like annular mode with the opposite polarity is observed in the extra-tropics (Fig. 3b). But the amplitudes are much weaker compared to those during the CP El Niño, especially for the anomalies in the subtropical belt.

To further estimate the symmetric and asymmetric components of the CP ENSO impacts, Fig. 3c, d depict the composite summation and difference of the 500-hPa geopotential height anomalies between the CP El Niño and CP La Niña. The symmetric component of the CP ENSO impact manifests an obvious AO-like annular mode response (Fig. 3d), whereas the asymmetric component is

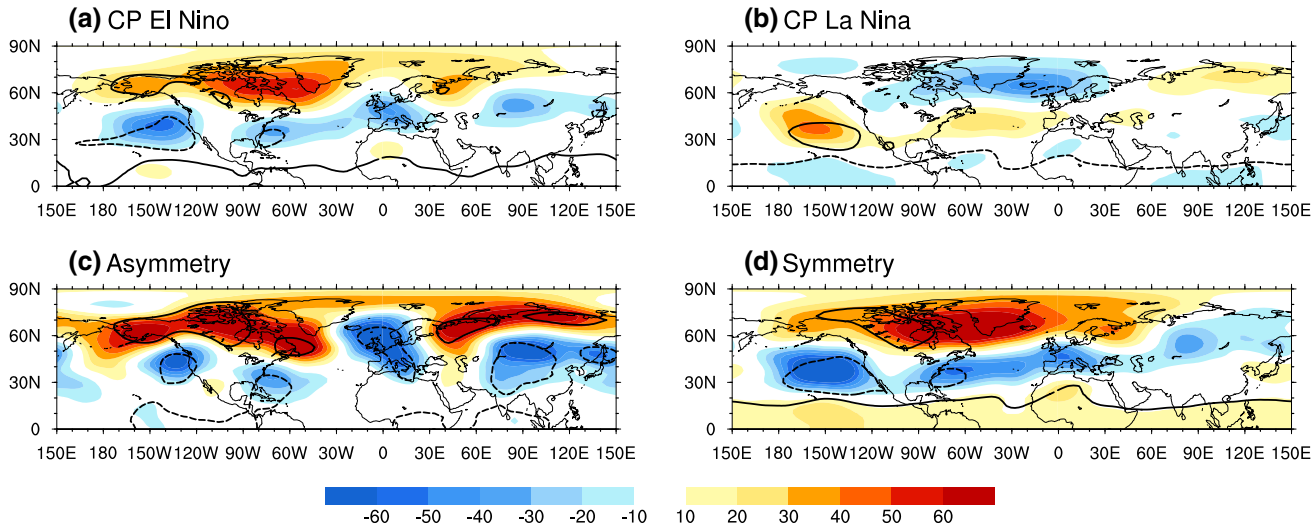

Fig. 3 Same as Fig. 2, but for the CP El Niño and CP La Niña cases

characterized by the strong negative height anomalies in most of the mid-latitudes and positive anomalies in most of the high latitudes (Fig. 3c). This asymmetry is a result of the stronger atmospheric responses to CP El Niño than CP La Niña, especially for the responses in the subtropical regions. Therefore, the atmospheric responses to CP ENSO manifest an evident asymmetric feature in amplitude, especially for the anomalies in the subtropical belt.

4 Possible physical mechanisms

4.1 EP ENSO

4.1.1 Establishment of the extra-tropical perturbation

The reasons responsible for the asymmetric impacts of ENSO on the climate anomalies inherently originate from the tropical forcing, while how the tropical forcing establishes the extra-tropical perturbation is a crucial process. As such, in order to make this issue clear, Fig. 4 depicts the distributions of the anomalous SST, 500 hPa *p*-vertical velocity and 200 hPa divergent winds for the EP El Niño and EP La Niña, respectively. Due to the short-term period of the outgoing longwave radiation (OLR), the anomalous 500 hPa *p*-vertical velocity is used to roughly represent the convective activity anomalies in the tropics. The warm SST anomalies during the EP El Niño are mainly located in the tropical central-eastern Pacific (Fig. 4a), which can trigger the enhanced convective anomalies and the associated anomalous upper-level divergence in the tropical Pacific (Fig. 4b). Thus, the poleward divergent winds are produced in the upper tropospheric region and confined to the domain of 170°E–130°W (Fig. 4b, vectors).

In contrast, during the EP La Niña, the negative SST anomalies are mainly found in the tropical central-eastern Pacific (Fig. 4d), showing a similar spatial pattern to the EP El Niño. The maximum of these negative SST anomalies is mainly located to the east of 150°W, which is consistent with a typical EP La Niña. Due to the asymmetric climatological SST distribution and the threshold of the occurrence of the convection, these negative SST anomalies induce much weaker convective anomalies in the tropical Pacific (Fig. 4e, shading) relative to the conditions during the EP El Niño. Then this suppressed convective anomaly induces the anomalous upper-level convergence in the tropical central Pacific (Fig. 4e, vectors). The associated equatorward convergent winds emerge, whereas they are much weaker than the anomalous poleward divergent winds during the EP El Niño.

In this process, compared with the EP El Niño, the EP La Nina is accompanied by a slightly westward shift of the tropical forcing anomalies. This asymmetry is a key factor that yields the shift of the PNA-like activity centers (Hoerling et al. 1997). Nevertheless, this westward shift is not as evident as that in the study of Hoerling et al. (1997), which is possibly because the CP La Niña events that have a positive contribution to the westward shift of the tropical forcing are excluded in this case. Thus, this weak westward shift of the tropical forcing anomalies causes a weak shift of the anomalous PNA-like activity centers.

The El Niño (La Niña)-induced upper-level tropical divergence (convergence) anomalies and the associated poleward divergent (equatorward convergent) wind anomalies would make a modification to the local Hadley circulation according to the mass balance law. This perturbation is crucial for the way the tropical forcing expands its impact to the extra-tropics as demonstrated by Simpkins et al. (2014). The modification in the local Hadley circulation is shown in Fig. 4c, f. The domain of the modified local Hadley circulation is identified according to the regions of the anomalous tropical forcing (170°E–130°W). Climatologically, this local Hadley circulation is characterized by the narrow ascending motion in the tropical region in the Northern Hemisphere and the descending motion in the subtropical region (Fig. 4c, shading). When the EP El Niño happens, the local Hadley circulation in the central-eastern Pacific is intensified by an anomalous meridional cell with the rising motion in the tropics and sinking motion in the subtropics (Fig. 4c, contours). Therefore, the local Hadley descending branch is substantially enhanced and expanded, and thereby the strong upper-level convergence is accompanied in the North Pacific (Fig. 4b, vectors). When the EP La Niña happens, the climatological local Hadley circulation is suppressed by the anomalous downward motion in the tropical region and anomalous upward motion in the subtropical region (Fig. 4f). Then the anomalous extra-tropical upper-level divergence is induced (Fig. 4e, vectors), but it is much weaker compared to that for the EP El Niño. Consequently, the perturbation of the local Hadley cell and the resultant subtropical upper-level divergent/convergent anomalies provide a bridge that the anomalous tropical forcing extends its influence to the extra-tropics, since these upper-level divergent/convergent anomalies likely play a vital role in determining the extra-tropical vorticity forcing anomalies (Simpkins et al. 2014).

In this process, although the intensity and location of the tropical SST anomalies are roughly similar between the EP El Niño and EP La Niña, the EP La Niña induces much weaker tropical forcing anomalies than the EP El Niño, including weaker convective anomalies and weaker upper-level convergent responses in the tropics. Correspondingly, the extra-tropical perturbations associated with EP La Niña, including the anomalous rising motion and the anomalous upper-level divergence, are also much weaker than those associated with EP El Niño. How this asymmetry induces

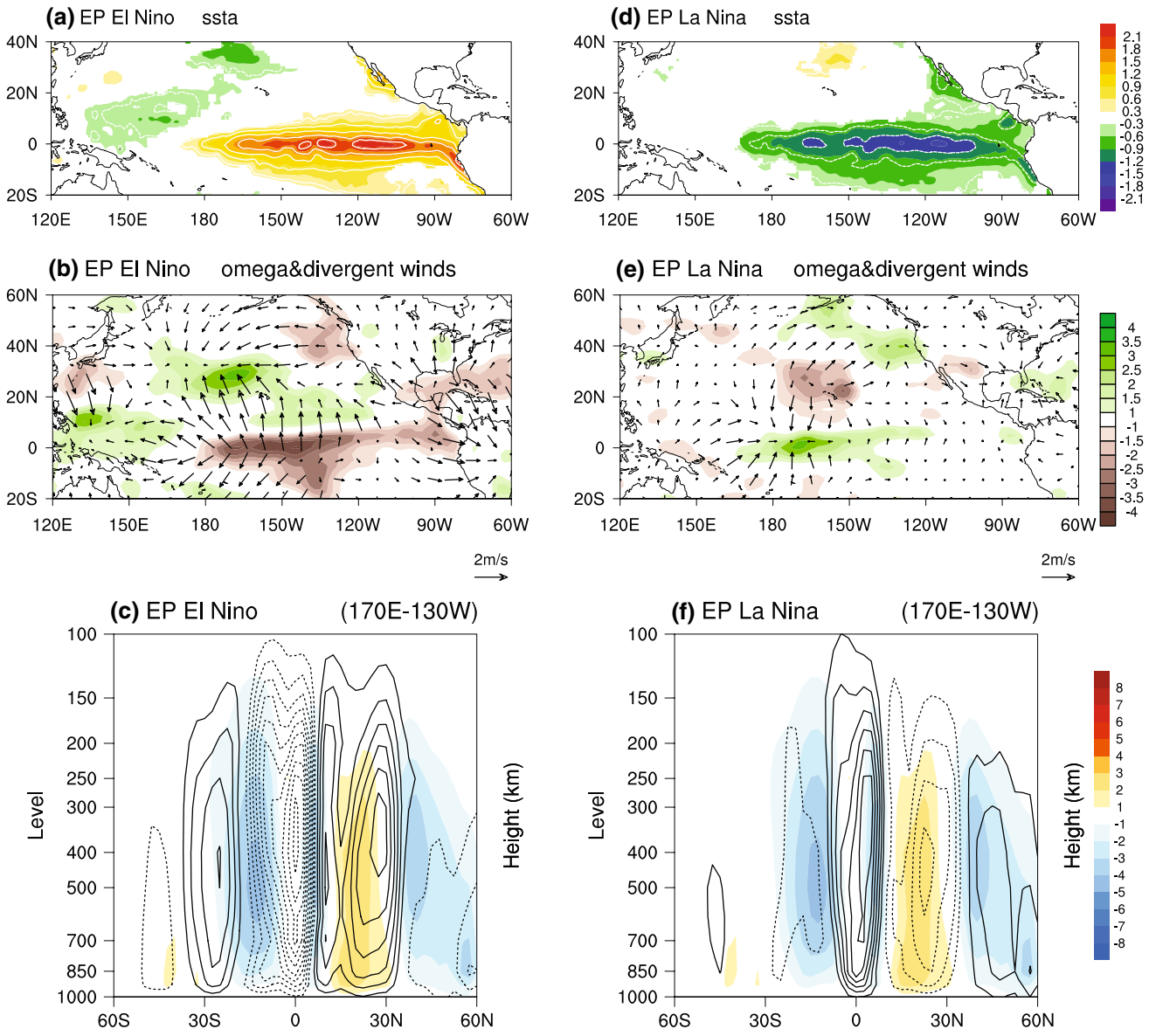

Fig. 4 The composite winter mean **a**, **d** SST anomalies (*shading*, °C), **b**, **e** 500 hPa *p*-velocity anomalies (*shading*, 10^{-2}Pa/s) superimposed by 200 hPa divergent wind anomalies (*vectors*, m/s) and **c**, **f** the local Hadley circulation anomalies are denoted by the vertical *p*-velocity anomalies averaged in the domain (170E−130 W) (*contours*, 10^{-2}Pa/s). The *shading* denotes the climatological local Hadley circulation. The *left column* is for the EP El Niño, and the *right column* for the EP La Niña. The SST and vertical *p*-velocity anomalies shown here are above the 95 % confidence levels

the extra-tropical asymmetric atmospheric responses is an important question, which will be discussed in the following section.

4.1.2 Rossby wave source

Whether the aforementioned extra-tropical upper-level divergent/convergent anomalies induced by the EP ENSO play a dominant role in the formation of the extra-tropical vorticity forcing? To answer this question, the Rossby wave source (RWS) is diagnosed according to Sardeshmukh and Hoskins (1988), which represents the generatioin of vorticity forcing. It is calculated from the barotropic vorticity equation at 200 hPa and the equation is as follows:

$$RWS = \underbrace{-\xi\nabla\cdot\bar{V}_x - \bar{\xi}\nabla\cdot V_x^{'}}_{vortex-stretching} \underbrace{-V_x^{'}\cdot\nabla\bar{\xi} - \bar{V}_x\cdot\nabla\xi^{'}}_{vorticity-advection} \quad (2)$$

where the $V_x^{'}$ and $\xi^{'}$ denote the anomalous upper-level divergent winds and absolute vorticity anomalies. The $\bar{V}_x$ and $\bar{\xi}$ signify the climatological divergent winds and absolute vorticity. The generation of the vorticity forcing (i.e. RWS)

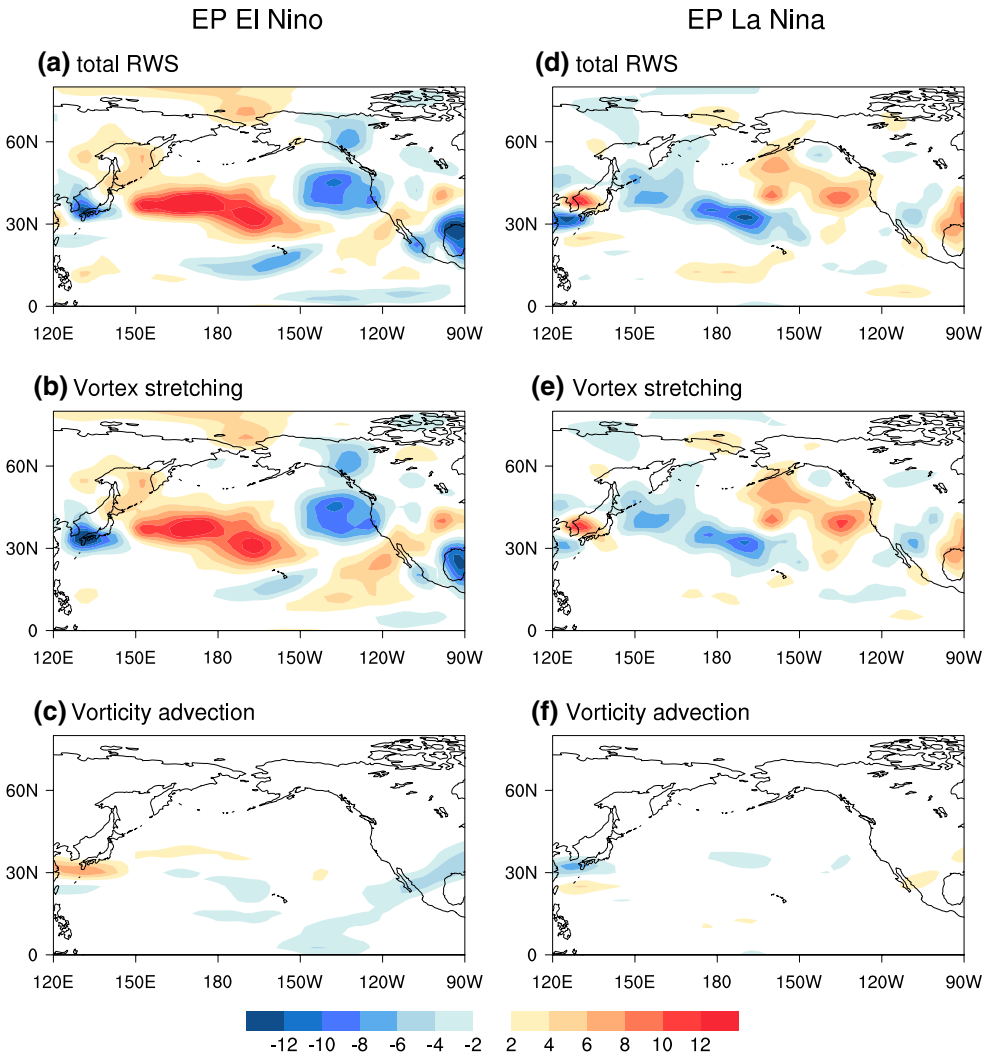

Fig. 5 The composite **a**, **d** total Rossby wave source, **b**, **e** vortex stretching and **d**, **f** vorticity advection anomalies (10^{-11} s^{-2}) for EP El Niño and EP La Niña, respectively

is determined by two terms: One is the vortex stretching that is related to the anomalous upper-level divergence and convergence. The other is the advection of vorticity associated with the anomalous divergent and convergent winds. To clarify which term plays a crucial role in the generation of the anomalous RWS, Fig. 5 shows the distributions of the anomalous total RWS, vortex stretching term and vorticity advection term during the EP El Niño and EP La Niña, respectively. The distrubiution of the vortex stretching component shows a strong similarity to the total RWS in both of the spatial pattern and intensity, while the vorticity advection part has a marginal contribution to the total RWS anomalies for both of EP El Niño and EP La Niña (Fig. 5). These results demonstrate that the anomalous RWS associated with the EP El Niño and EP La Niña predominantly depends on the vortex stretching term. In other words, the extra-tropical upper-level divergent/convergent anomalies, induced by the modulated local Hadley circulation, dominatly determine the generation of the extra-tropical anomalous vorticity forcing.

Specifically, during the EP El Niño, the positive RWS belt are oriented northwest-southeast in the subtropical central and eastern Pacific, matching the intensified descending branch of the local Hadley circulation and the related extra-tropical convergent anomalies (Fig. 5a). In contrast, during the EP La Niña, the negative RWS anomalies oriented northwest–southeast are narrower and weaker relative to the conditions during the EP El Niño (Fig. 5d). These extra-tropical vorticity forcing anomalies are associated with the generation of the PNA-like teleconnection. The stronger RWS anomalies associated with the EP El Niño favor a stronger PNA-like teleconnection. Thus, the asymmetry in the anomalous RWS intensity between the EP El Niño and EP La Niña tends to induce the amplitude asymmetry in the PNA-like teleconnection.

4.1.3 Wave propagation and wave ray trajectory

To further dig out the reasons responsible for the EP ENSO-induced atmospheric asymmetry, the wave activity flux is

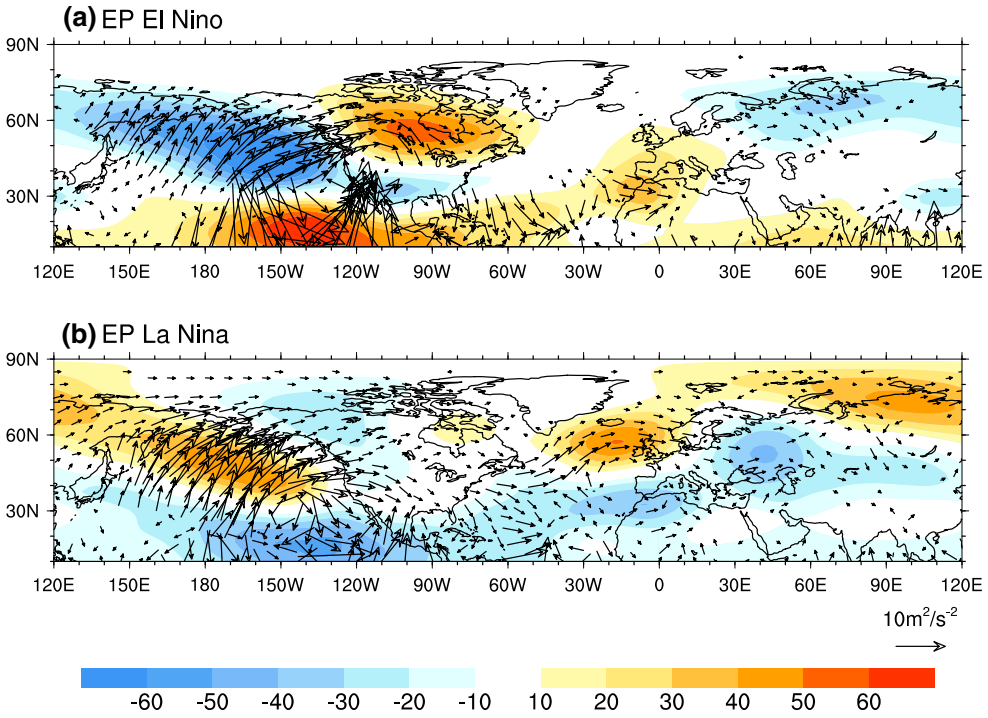

Fig. 6 The composite 200 hPa wave activity flux (*vectors*) and 200 hPa geopotential height anomalies (*shading*, gpm) for the **a** EP El Niño and **b** EP La Niña, respectively. The *vectors* less than 0.5 $m^2\ s^{-2}$ are omitted

diagnosed based on the Eq. (1) to explore the extra-tropical Rossby wave propagation. Figure 6 gives the composite 200 hPa wave activity flux and 200 hPa geopotential height anomalies for the EP El Niño and EP La Niña, respectively. Over the Pacific–North American region, an obvious wave activity flux induced by the EP El Niño originates from the anomalous RWS (i.e. North Pacific), and propagates northeastward and finally penetrates into the central–western part of the North America, which is consistent with the PNA-like teleconnection (Fig. 6a). Subsequently, the wave activity flux turns equatorward into the tropical Atlantic. Over the North Atlantic–Eurasian region, the wave activity flux is much weaker, corresponding to the weak responses of the geopotential height anomalies (Fig. 6a, shading).

In contrast, during the EP La Niña, the wave activity flux emerging from the North Pacific propagates northeastward into the west coast of the North America, and then disappears instead of penetrating into the eastern part of the North America. This wave activity flux corresponds to the westward shift of the geopotential height anomalies over the North America produced by the EP La Niña. Moreover, the wave activity flux triggered by the EP La Niña splits into another direction over the west coast of the North America. It penetrates into Atlantic and further reaches the Eurasian continent. This prominent wave activity flux signal is in accordance with the Atlantic–Eurasian teleconnection associated with EP La Niña (Fig. 6b).

The wave activity flux shows a prominent asymmetry between the EP El Niño and EP La Niña, which is in concert with the asymmetry in the geopotential height anomalies. Moreover, it is known that the background flows play an important role in the wave propagation. Therefore, we diagnosed the wave ray trajectory to examine the impact of the background flows on the wave propagation. On the basis of the linearized barotropic non-divergent vorticity equation, the dispersion relation describing the perturbation propagation is obtained on a time-mean slowly varying basic state with the WKB approximation (e.g., Karoly 1983; Li and Nathan 1997; Li and Li 2012; Li et al. 2015; Zhao et al. 2015) as

$$\varpi = \bar{u}_M k + \bar{v}_M l + \frac{\bar{q}_x l - \bar{q}_y k}{k^2 + l^2}, \tag{3}$$

where $\bar{q}_x$, $\bar{q}_y$ are the zonal and meridional gradient of climatological state absolute vorticity, $(\bar{u}_M, \bar{v}_M)$ are the zonal and meridional component of the climatological flows under Mercator projection. The climatological state is defined by the anomalies induced by El Niño/La Niña plus the long-term mean derived from reanalysis data spanning the period from 1950 to 2011. k, l, ϖ denote the zonal wavenumber, meridional wavenumber and the angular frequency, respectively. The wavenumber for the stationary waves is defined as

$$K^2 = \frac{\bar{q}_y k - \bar{q}_x l}{\bar{u}_M k + \bar{v}_M l} \tag{4}$$

The zonal and meridional components of group velocity take the form

$$u_g = \frac{\partial \varpi}{\partial k} = \bar{u}_M + \frac{(k^2 - l^2)\bar{q}_y - 2kl\bar{q}_x}{K^4}, \tag{5}$$

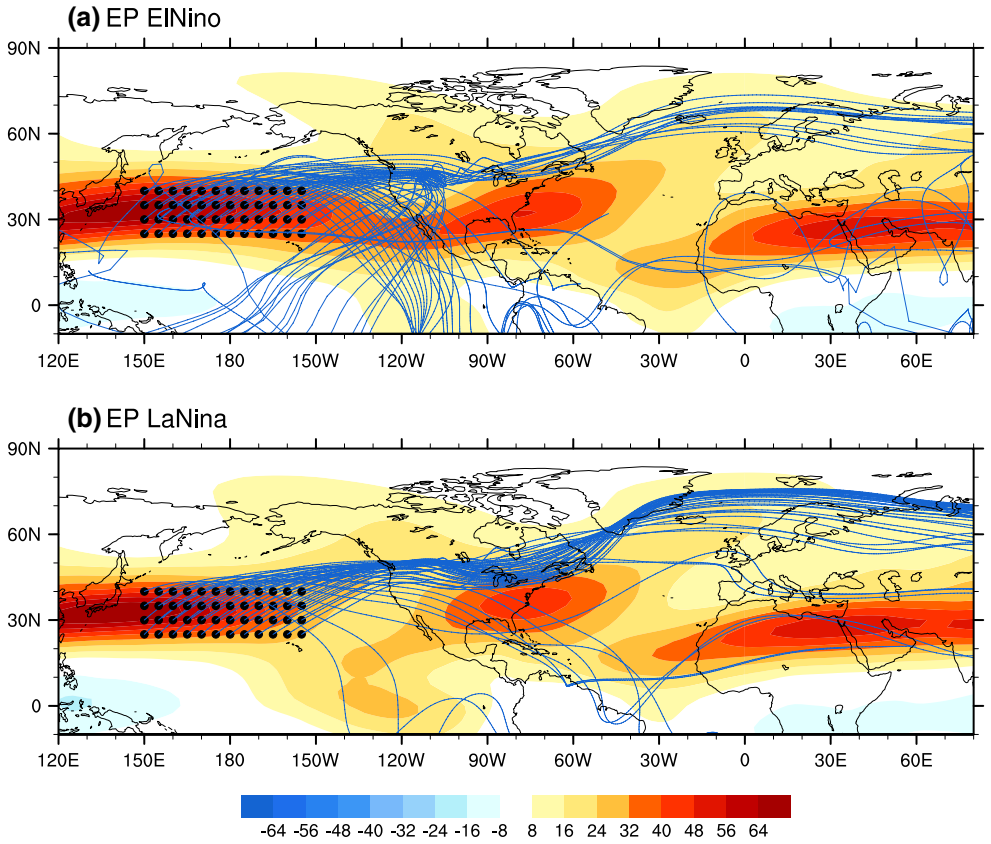

Fig. 7 The wave ray trajectory with the initial zonal wavenumber 4 and initial positive meridional wavenumber l under the background state of **a** the EP El Niño and **b** EP La Niña, respectively. The *shading* denotes the background zonal winds for the EP El Niño and EP La Niña, respectively (unit, m/s). The initial latitudes and longitudes are given based on the RWS anomalies (*black dots*)

$$v_g = \frac{\partial \varpi}{\partial l} = \bar{v}_M + \frac{(k^2 - l^2)\bar{q}_x + 2kl\bar{q}_y}{K^4} \tag{6}$$

Both l and k vary along the ray paths due to the varying longitudinal and latitudinal basic state. Their evolution depends on the kinematic wave theory (Whitham 1960) as follows:

$$\frac{d_g k}{dT} = -\frac{\partial \varpi}{\partial X} = -k\frac{\partial \bar{u}_M}{\partial X} - l\frac{\partial \bar{v}_M}{\partial X} - \frac{1}{K^2}\left(l\frac{\partial \bar{q}_x}{\partial X} - k\frac{\partial \bar{q}_y}{\partial X}\right), \tag{7}$$

$$\frac{d_g l}{dT} = -\frac{\partial \varpi}{\partial Y} = -k\frac{\partial \bar{u}_M}{\partial Y} - l\frac{\partial \bar{v}_M}{\partial Y} - \frac{1}{K^2}\left(l\frac{\partial \bar{q}_x}{\partial Y} - k\frac{\partial \bar{q}_y}{\partial Y}\right), \tag{8}$$

where $\frac{d_g}{dT} = \frac{\partial}{\partial T} + u_g\frac{\partial}{\partial X} + v_g\frac{\partial}{\partial Y}$ indicates the Lagrangian variation moving at the group velocity. Thus, the ray trajectory can be derived through integrating the Eqs. (5–8) after the basic state, the initial latitude and longitude and the initial zonal wavenumber are given. In this study, the initial zonal wavenumber is given by 4, and the initial meridional wavenumber is derived by solving the cubic Eq. (4). Here, the positive initial meridional wavenumber is chosen, since most wave rays with the negative meridional wavenumber propagate into the Southern Hemisphere. Before the calculation of the wave ray, the basic states of the zonal and meridional winds are smoothed through two-dimensional Fourier series truncated at wavenumber 5. The calculation is terminated after the wavenumbers larger than 40.

Figure 7 gives the wave ray trajectory under the background states of the EP El Niño and EP La Niña, respectively. The results shown here are only for the positive initial meridional wavenumber l. The initial latitudes and longitudes are set in the mid-latitudes based on the location of the EP ENSO-related RWS anomalies (Fig. 7a, b). Here, we chose the same initial latitudes and longitudes for both of EP El Niño and EP La Niña so that it is better to compare the roles of the different background states in the wave activity. Multiple launch points are chosen in order to better reflect the impacts of the background state on the wave propagation. Under the background state of the EP El Niño, most of the wave rays are unable to penetrate into the North Atlantic, but they turn equatorward instead (Fig. 7a). Therefore, the EP El Niño background state tends to confine the wave activity

to the Pacific–North American region, consistent with the significant geopotential height anomalies over the Pacific–North American region but weak anomalies over the Atlantic–Eurasian region. In contrast, when the background state is changed into the EP La Niña condition, nearly all the wave rays are able to propagate far into the Eurasian continent (Fig. 7b), favoring the formation of the Atlantic–Eurasian teleconnection. Consequently, the EP La Niña background state is more conducive to the Rossby wave propagation in the Northern Hemisphere than the EP El Niño background state, especially over the Atlantic–Eurasian regions. As a result, the different effects of the warm and cold EP ENSO background states on the wave propagation are primarily responsible for the asymmetry in the extra-tropical atmospheric responses, especially over the Atlantic–Eurasian region. In addition, the wave ray trajectories with the initial zonal wavenumber 2 and 3 are also calculated. We found that more wave rays turn equatorward before they reach the far Eurasia during the EP El Niño-type state than the EP La Niña-type state (Figure not shown). However, this asymmetric feature is not as significant as that in Fig. 7. Thus, the results from the zonal wavenumber 4 are much more consistent with the observational results and mainly responsible for the asymmetry of the circulation anomalies.

4.2 CP ENSO

4.2.1 Establishment of the extra-tropical perturbation

It is known that the CP ENSO is characterized by a completely different anomalous SST pattern (as shown in Fig. 1), thereby establishing a distinct anomalous tropical forcing and the associated extra-tropical perturbation. The characteristics of the anomalous SST, 500 hPa *p*-vertical velocity and 200 hPa divergent winds related to the cold and warm CP ENSO are given in Fig. 8. The CP El Niño is featured by the positive SST anomalies located in the tropical central Pacific, while the CP La Niña is featured by the slightly stronger negative SST anomalies. Nevertheless, the maximum of the SST anomalies for the two events is located in a similar region (about 180°–150°W) (Fig. 8a, d). Correspondingly, the anomalous convective activity in the tropics induced by the CP El Niño and CP La Niña presents a similar spatial pattern and location (Fig. 8b, e; shading). Only the maximum convective anomalies shift a little westward during the cold CP ENSO due to the asymmetry in the climatologically zonal SST distribution. Subsequently, these diabatic heating (cooling) anomalies induce the upper-level anomalous divergence (convergence) in the tropical central Pacific during the CP El Niño (La Niña), which forces the corresponding poleward (equatorward) divergent (convergent) wind anomalies in the domain of 150°E–150°W (Fig. 8b, e; vectors).

According to the mass balance law, an anomalous meridional circulation will be generated and then the local Hadley circulation will be perturbed around the central Pacific for both of CP El Niño and CP La Niña as shown in Fig. 8c, f. Climatologically, this local Hadley circulation is characterized by the powerful ascending branch in the tropics and descending branch in the subtropics (Fig. 8c, f, shading). When a CP El Niño happens, an anomalous meridional cell is established with the ascending motion in the tropics and descending motion in the subtropics (Fig. 8c, contours), thereby intensifying the local Hadley circulation. In contrast, during the CP La Niña, a reverse anomalous meridional cell with the descent in the tropics and ascent in the subtropics is observed, which weakens the local Hadley circulation (Fig. 8f, contours). All these tropical forcing anomalies and the related perturbed local Hadley cell during the CP ENSO move westward relative to those during the EP ENSO. This westward shift of the tropical and extra-tropical forcing favors the formation of the AO-like teleconnection during the CP ENSO. Jia et al. (2009) suggested that when the tropical forcing moves to the west of the tropical central Pacific, the atmospheric responses tend to change from the PNA-like to AO-like pattern. This difference is already discussed by previous studies (Graf and Zanchettin 2012; Jia et al. 2009; Li et al. 2006). In this study however, we mainly put our focus on the asymmetric impacts between the CP (EP) El Niño and CP (EP) La Niña.

4.2.2 Rossby wave source

Whether the anomalous upper-level convergence/divergence in the subtropical Pacific during the CP ENSO predominantly determines the extra-tropical anomalous vorticity forcing just as the conditions during the EP ENSO? In order to answer this question, the anomalous RWS and its respective vortex stretching and vorticity advection component are calculated according to the Eq. (2) during the CP El Niño and CP La Niña (Fig. 9). The distribution and intensity of the anomalous vortex stretching part shows a close similarity to the total RWS anomalies for both of CP El Niño and CP La Niña, indicating that this part plays a decisive role in the formation of the RWS anomalies. Therefore, it can be concluded that the anomalous upper-level subtropical divergence/convergence, as a result of the perturbation of the local Hadley circulation, induces the extra-tropical anomalous vorticity forcing through the vortex stretching effect. Thus, the anomalous tropical forcing is "transmitted" to the extra-tropics.

Specifically, during the CP El Niño, a positive RWS belt is oriented northeast-southwest (Fig. 9a), while a similar negative RWS belt is seen in the subtropical Pacific during the CP La Niña (Fig. 9d). Compared with the anomalous

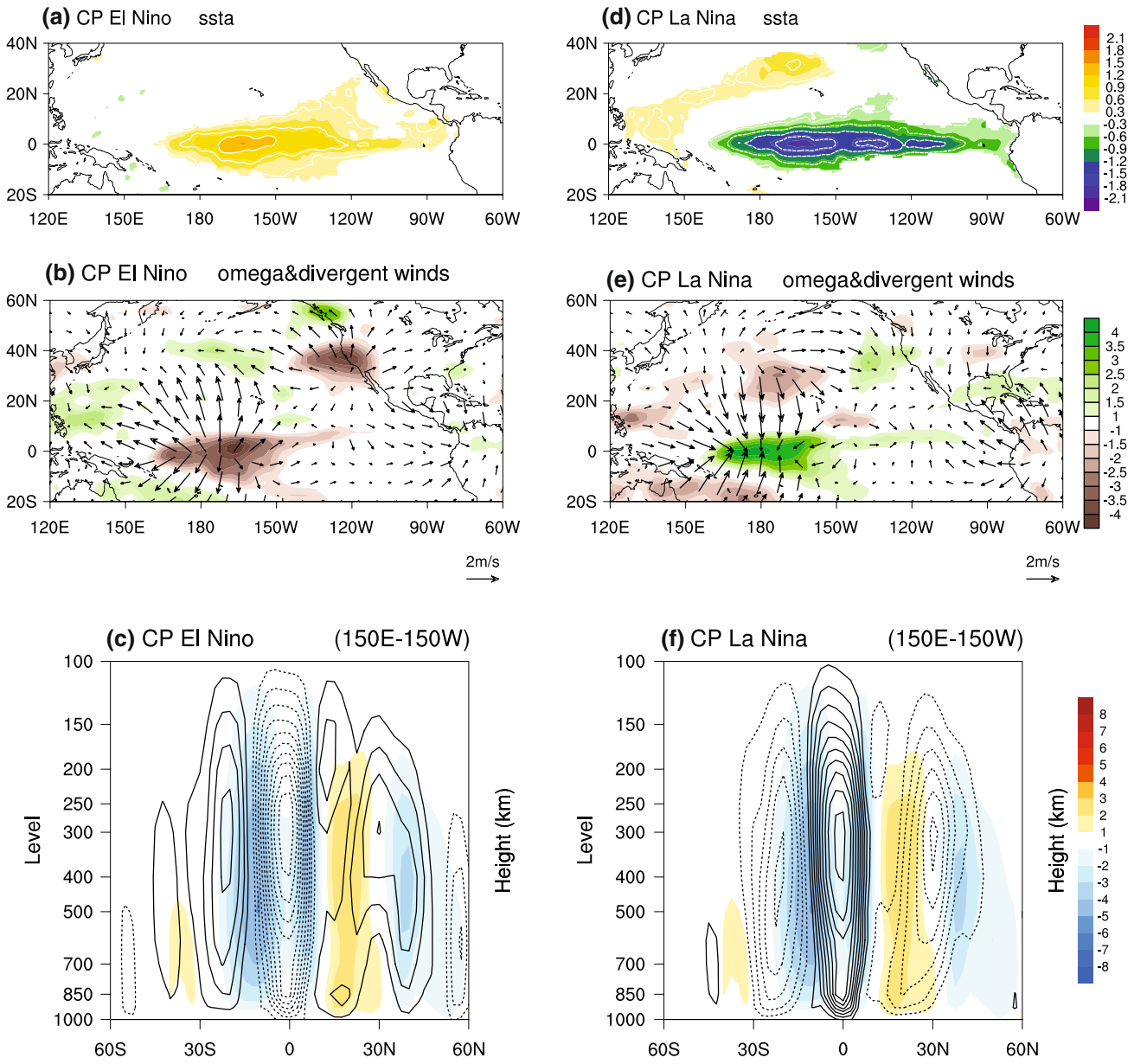

Fig. 8 Same as Fig. 4, but for the CP El Niño and CP La Niña conditions

RWS during the EP ENSO, the anomalous RWS during the CP ENSO shows a much weaker asymmetry. Moreover, the process of the establishment of the extra-tropical perturbation also shows a weaker asymmetry as discussed in Fig. 8. These results indicate that these physical processes do not dominantly account for the asymmetric atmospheric responses to the CP El Niño and CP La Niña.

4.2.3 Wave propagation and wave ray trajectory

To further make clear the reasons of the asymmetric impacts of CP ENSO, the 200 hPa Rossby wave activity flux is shown in Fig. 10, examining the propagation of the Rossby waves. In the case of CP El Niño, the Rossby wave activity flux originating from the North Pacific spreads into two directions (Fig. 10a, vectors). One is equatorward. This branch penetrates into the North Atlantic, and continues to propagate into Eurasia, which is consistent with the prominent AO-like teleconnection. The other is northeastward, but this branch is weak and finally seems to merge with the equatorward branch over the North Atlantic. In the case of CP La Niña, the wave activity flux originating from the North Pacific propagates northeastward and subsequently it weakens. In this case, the wave train structure

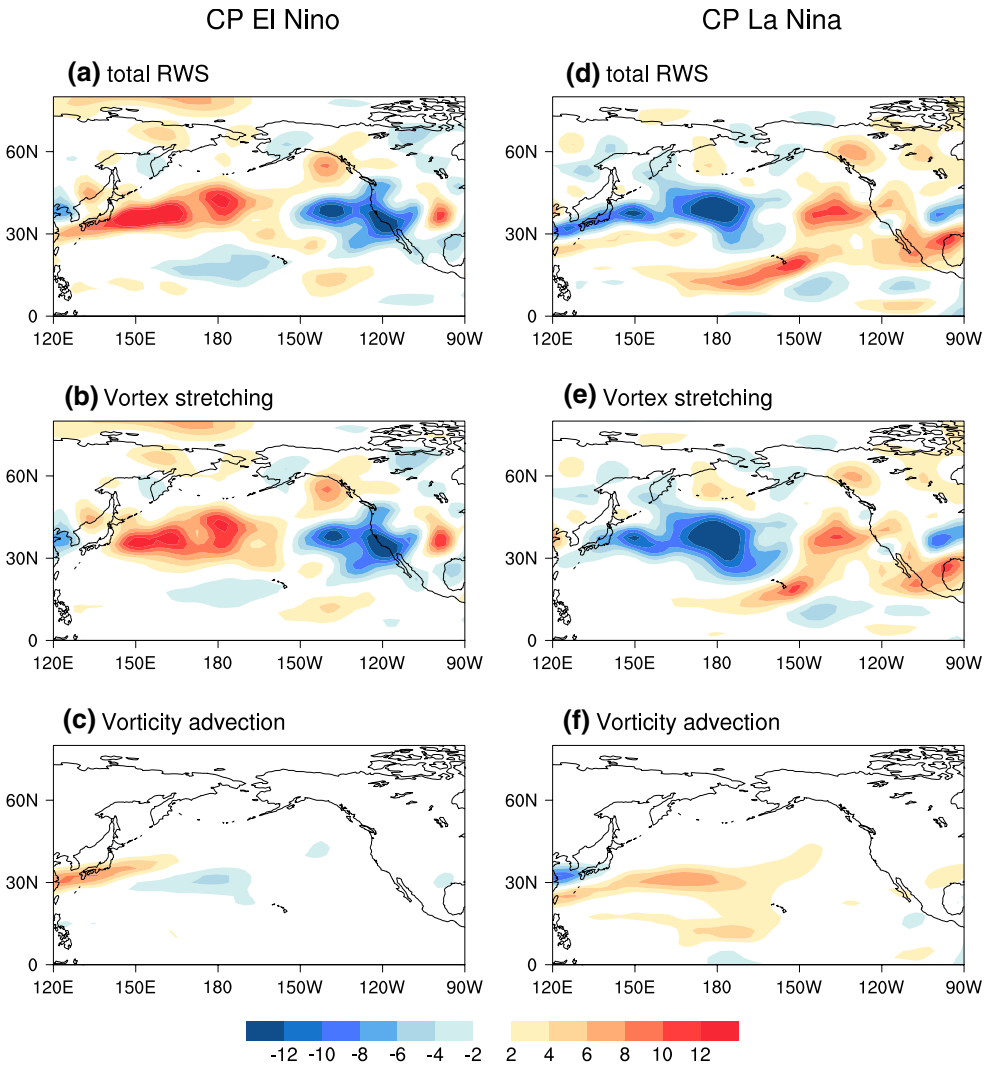

Fig. 9 The composite **a**, **d** total Rossby wave source, **b**, **e** vortex stretching and **d**, **f** vorticity advection anomalies (10^{-11} s^{-2}) for CP El Niño and CP La Niña, respectively

is not obvious. Thus, the wave activity flux manifests an obviously different feature between the CP El Niño and CP La Niña.

Due to the important roles of the background state in the Rossby wave propagation, furthermore, the wave ray trajectory is diagnosed according to the Eqs. (3–8) under the CP El Niño-type and CP La Niña-type basic states, respectively (Fig. 11). The multiple launch points are chosen in the subtropical region based on the anomalous RWS associated with CP El Niño. Here, the same launch points are chosen for both of the warm and cold CP ENSO in order to better highlight the roles of the background state. The results for the negative initial meridional wavenumber l are shown here (Fig. 11a, b), while results for the positive meridional wavenumber are not shown because the ray trajectories east of 90°W are resemble between CP El Niño and CP La Niña, which is not responsible for the asymmetry of the subtropical circulation anomalies. In addition, fewer wave rays can propagate downstream with the initial zonal wavenumber 2 and 3 (Figure not shown), which is inconsistent with the observational results. Thus, the initial zonal wavenumber 4 is chosen. Under the CP El Niño background state, two branches of the wave ray trajectory are found: One is poleward. The other is equatorward. The equatorward branch is reflected at the latitudes where the zonal winds equal zero (U = 0), and then the trajectory is trapped in the subtropical westerly jet. This is possibly because of the strong enhancement of the subtropical westerly jet induced by the CP El Niño. In contrast, under the CP La Niña background state, the wave ray trajectory is mainly poleward, corresponding to the obvious geopotential height anomalies in the high latitudes. The equatorward branch disappears at U = 0 latitudes and cannot be captured by the subtropical westerly jet. Therefore, the prominent difference in the equatorward branch seems responsible for the strong asymmetric subtropical belt of the AO-like teleconnection between the CP El Niño and CP La Niña.

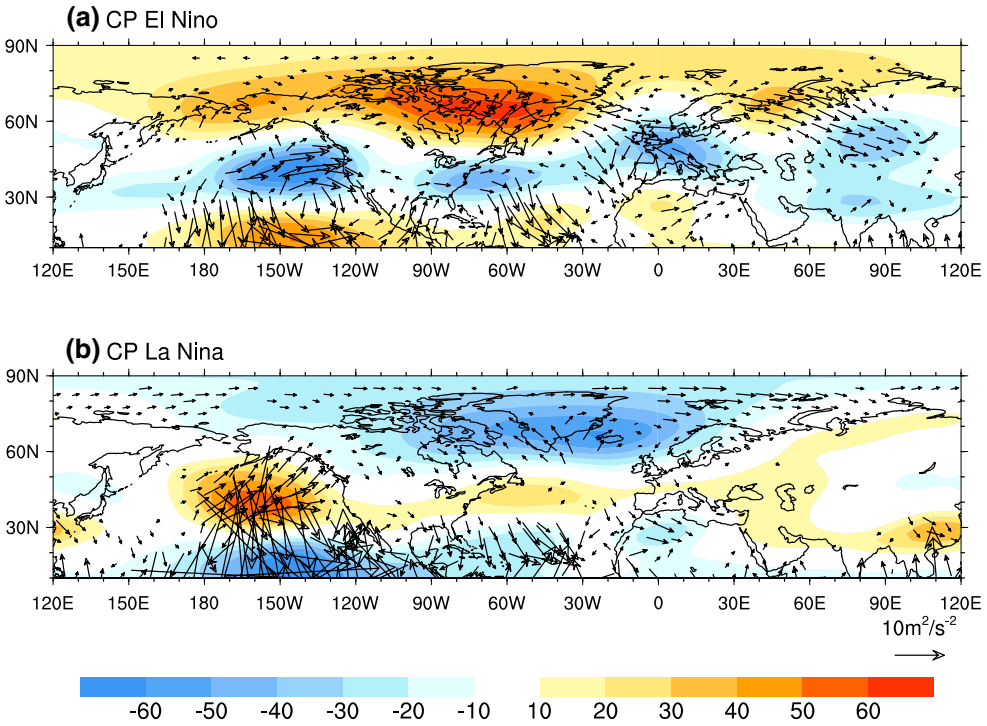

Fig. 10 The composite 200 hPa wave activity flux (*vectors*, $m^2\ s^{-2}$) and 200 hPa geopotential height anomalies (*shading*, gpm) for the **a** CP El Niño and **b** CP La Niña, respectively. The *vectors* less than 0.5 $m^2\ s^{-2}$ are omitted

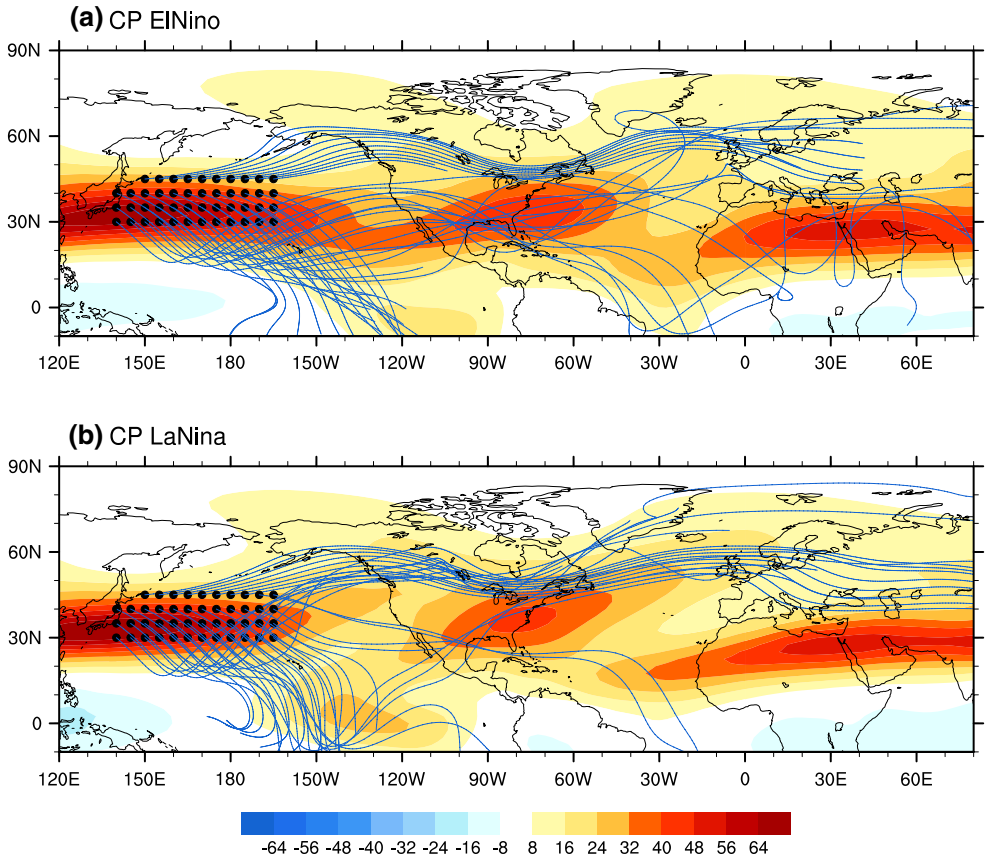

Fig. 11 The wave ray trajectory with the initial zonal wavenumber 4 and negative initial meridional wavenumber *l* under the background state of **a** the CP El Niño and **b** CP La Niña (*blue contours*), respectively. The *shading* denotes the background zonal winds for the CP El Niño and CP La Niña, respectively (unit, m/s). The initial latitudes and longitudes are given based on the RWS anomalies (*black dots*)

Previous results insisted that the La Niña-type background state is much more in favor of the Rossby wave propagation than the El Niño-type state (Lin and Derome 2004). This situation just occurs for the EP ENSO. However, for the CP ENSO, the CP El Niño-type background state tends to be more conducive to the Rossby wave propagation.

5 Conclusions and discussions

In this study, we revisited the asymmetric impacts of ENSO on the Northern Hemisphere winter atmospheric circulation through classifying ENSO into two types: EP ENSO and CP ENSO. Some new interesting results are acquired after this classification. The results demonstrate that the EP ENSO triggers two obvious asymmetric atmospheric teleconnections: One is the PNA-like teleconnection. The other is the Atlantic–Eurasian teleconnection with the negative height anomalies in the subtropical Atlantic and Eurasian continent and positive anomalies in the high-latitude Atlantic and northeast Asia. The asymmetry of the former teleconnection is dominantly characterized by the weaker amplitudes during the EP La Niña than EP El Niño. However, the latter teleconnection shows a much more prominent asymmetry, which only appears during the EP La Niña but not during the EP El Niño.

In contrast, the atmospheric teleconnection associated with CP ENSO presents completely different features from the EP ENSO, showing an AO-like teleconnection in the extra-tropics for both of CP El Niño and CP La Niña. Although the AO-like teleconnection manifests a similar spatial pattern just with the opposite polarity between the CP El Niño and CP La Niña, this annular mode shows an appreciable asymmetry in the subtropical amplitude that is stronger during the CP El Niño than during the CP La Niña.

To further dig out the physical reasons responsible for these asymmetric atmospheric responses, firstly, the way the tropical SST anomalies establish the extra-tropical anomalous vorticity forcing is investigated, which is closely related to the generation of the extra-tropical atmospheric anomalies. The tropical Pacific SST anomalies for both of EP ENSO and CP ENSO induce the convective anomalies in the tropical Pacific, which further triggers the upper-level anomalous divergence/convergence in the tropics through releasing the latent heat. Then the upper-level divergent/convergent winds are emanated from the tropics. According to the mass balance law, the local Hadley circulation is perturbed. Subsequently, the anomalous upper-level divergence/convergence is formed in the subtropics, which dominantly determines the generation of the extra-tropical anomalous vorticity forcing through producing the vortex stretching effect. This physical process is in accordance with that proposed by Simpkins et al. (2014). They analyzed the impacts of the tropical Atlantic SST anomalies on the extra-tropical atmospheric circulation in the Southern Hemisphere. Although the established physical process of the extra-tropical vorticity forcing is the same for both of EP and CP ENSO, the vorticity forcing presents diverse features for different types and phases of ENSO, further leading to distinct asymmetric atmospheric teleconnections.

In the case of the EP ENSO, compared with the EP El Niño, the EP La Niña yields a weaker tropical anomalous forcing, such as weaker anomalous convective activities and weaker tropical upper-level convergent anomalies, and subsequently causes the corresponding weaker extra-tropical perturbations including the extra-tropical divergent anomalies and the RWS anomalies. Thus, a much weaker PNA-like teleconnection is produced by the EP La Niña. In terms of the asymmetric Atlantic–Eurasian teleconnection, the effects of the background state on the Rossby wave propagation play a vital role. As such, the wave ray trajectory is diagnosed. The same multiple launch points are chosen for both of the EP El Niño and EP La Niña to highlight the roles of the background flow. Under the background state of the EP El Niño, it is difficult for the Rossby wave rays to propagate into the Atlantic region. However, when the background state is changed into the EP La Niña condition, most of the wave rays are able to penetrate far into the Eurasian continent, favoring the establishment of the Atlantic–Eurasian teleconnection. Thus, the sensitivity of the Rossby wave propagation to the background state causes the robust asymmetric impacts of the EP ENSO on the Atlantic–Eurasian teleconnection.

However, the results on the roles of the background state in the ENSO induced-PNA-like pattern are still inconsistent. For example, according to a barotropic numerical model, Hoerling et al. (1997) insisted that the PNA-like response to El Niño and La Niña could be successfully captured no matter whether the model is linearized about the zonal flow of El Niño or La Niña. Other authors suggested that small changes in the background state could induce a significant variation in the atmospheric responses (Ting and Sardeshmukh 1993; Hall and Derome 2000).

In the case of the CP ENSO, both of the tropical anomalous forcing and the extra-tropical perturbations present a similar spatial pattern and intensity between the cold and warm CP ENSO, showing a weak asymmetry. Therefore, these physical signals are unable to explain the asymmetry in the AO-like teleconnection triggered by the CP ENSO. Further studies found that the different background states between the CP El Niño and CP La Niña effectively impact

the wave propagation. On the one hand, the results demonstrate that there exist obvious poleward wave ray trajectories in the high latitudes for both of the CP El Niño-type and CP La Niña-type background states. This favors the formation of the geopotential height anomalies in the high latitudes of the Northern Hemisphere, which is consistent with the strong positive geopotential height anomalies for the CP El Niño and negative anomalies for the CP La Niña. On the other hand, the equatorward wave rays present totally different trajectories for the different basic states. Under the CP El Niño background state, the wave rays are reflected at $U = 0$ latitudes, and then are successfully captured by the subtropical westerly jet. However, when the background state is changed into the CP La Niña condition, the equatorward wave rays disappear at $U = 0$. This difference explains why the geopotential height anomalies in the subtropics are strong and significant during the CP El Niño but not during the CP La Niña.

Many previous studies indicated that the impact of ENSO on the Euro-Atlantic atmospheric circulation (EAAC) is uncertain and non-stationary (Bronnimann 2007; Dong et al. 2000; Greatbatch et al. 2004). The correlation between ENSO and the EAAC is insignificant in the long-term period due to their complicated relationship. Greatbatch et al. (2004) found that the impact of ENSO on the EA winter climate is weak for the period from 1957 to 1977 and robust from 1978 to 1997. López-Parages et al. (2015) reported that although the tropical forcing associated with El Niño is roughly similar for different interdecadal periods, the El Niño-EAAC relationship is still able to show distinct features. They further demonstrated that such a result is caused by the different mean state conditions that impact the propagation of the Rossby waves. In this study, when the same mean state is added to the EP (CP) El Nino and EP (CP) La Nina anomalies, respectively, the extra-tropical Rossby waves show substantially different features, especially over the Atlantic–Eurasian region, finally inducing the asymmetric impacts of EP (CP) El Niño and EP (CP) La Niña on the EAAC. This asymmetric impact makes a great contribution to the insignificant ENSO–EAAC relationship that revealed by previous studies (Bronnimann 2007; Dong et al. 2000; Greatbatch et al. 2004). Moreover, the ENSO–EAAC relation diverges after ENSO is divided into two types, which also tends to yield an unclear ENSO–EAAC relationship. Thus, this work is beneficial to accurately predict the Euro–Atlantic climate using the most significant tropical signal (i.e. ENSO).

Acknowledgments We thank for the valuable comments and suggestions from the reviewers, which have led to a significant improvement of this paper. This study is supported by the National Natural Science Foundation of China (Grant Nos. 41230527, 41461164005 and 41461144001).

References

Ashok K, Yamagata T (2009) The El Niño with a difference. Nature 461:24

Ashok K, Behera SK, Rao SA, Weng H, Yamagata T (2007) El Niño Modoki and its possible teleconnection. J Geophys Res 112:C11007. doi:10.1029/2006JC003798

Bronnimann B (2007) Impact of El Nino–Southern Oscillation on European climate. Rev Geophys 45:RG3003. doi:10.1029/2006RG000199

Cai W, Rensch PV, Cowan T, Sullivan A (2010) Asymmetry in ENSO teleconnection with regional rainfall, its multidecadal variability, and impact. J Clim 23:4944–4955

Chowdary JS, Xie SP, Tokinaga H, Okumura YM, Kubota H, Johnson N, Zheng XT (2012) Interdecadal variations in ENSO teleconnection to the Indo–Western Pacific for 1870–2007. J Clim 25:1722–1744

Coelho CAS, Goddard L (2009) El Nino-induced tropical droughts in climate change projections. J Clim 22:6456–6476

Deser C, Wallace JM (1990) Large-scale atmospheric circulation features of warm and cold episodes in the tropical Pacific. J Clim 3:1254–1281

Dong BW, Sutton RT, Jewson SP, O'Neill A, Slingo JM (2000) Predictable winter climate in the North Atlantic sector during the 1997–1999 ENSO cycle. Geophys Res Lett 27:985–988

Feng J, Wang L, Chen W, Fong SK, Leong KC (2010) Different impacts of two types of Pacific ocean warming on Southeast Asian rainfall during boreal winter. J Geophys Res. doi:10.1029/2010JD014761

Feng J, Chen W, Tam CY, Zhou W (2011) Different impacts of El Nino and El Nino Modoki on China rainfall in the decaying phases. Int J Climatol 31:2091–2101

Frauen C, Dommenget D, Tyrrell N, Rezny M, Wales S (2014) Analysis of the nonlinearity of El Nino–Southern oscillation teleconnections. J Clim 27:6225–6244

Garfinkel CL, Hurwitz MM, Waugh DW (2013) Are the teleconnections of Central Pacific and Eastern Pacific El Nino distinct in boreal wintertime? Clim Dyn 41:1835–1852

Gershunov A, Barnett TP (1998) Interdecadal modulation of ENSO teleconnections. Bull Am Meteorol Soc 79:2715–2725

Graf HF, Zanchettin D (2012) Central Pacific El Nino, the "subtropical bridge", and Eurasian climate. J Geophys Res. doi:10.1029/2011JD016493

Greatbatch RJ, Lu J, Peterson KA (2004) Nonstationary impact of ENSO on Euro–Atlantic winter climate. Geophys Res Lett 31:L02208. doi:10.1029/2003GL018542

Hall NMJ, Derome J (2000) Transience, nonlinearity, and eddy feedback in the remote response to El Nino. J Atmos Sci 57:3992–4007

Hannachi A (2001) Toward a nonlinear identification of the atmospheric response to ENSO. J Clim 14:2138–2149

Hoerling MP, Kumar A, Zhong M (1997) El Nino, La Nina, and the nonlinearity of their teleconnections. J Clim 10:1769–1786

Hoerling MP, Kumar A, Xu TY (2001) Robustness of the nonlinear climate response to ENSO's extreme phases. J Clim 14:1277–1293

Horel JD, Wallace JM (1981) Planetary-scale atmospheric phenomena associated with the southern oscillation. Mon Weather Rev 109:813–829

Jia XJ, Lin H, Derome J (2009) The influence of tropical Pacific forcing on the Arctic Oscillation. Clim Dyn 32:495–509

Kalnay E et al (1996) The NCEP/NCAR 40-year reanalysis project. Bull Am Meteorol Soc 77:437–471

Kao HY, Yu JY (2009) Contrasting eastern-Pacific and central-Pacific types of ENSO. J Clim 22:615–632

Karoly DJ (1983) Rossby wave propagation in a barotropic atmosphere. Dyn Atmos Oceans 7:111–125

Karori MA, Li J, Jin FF (2013) The asymmetric influence of the two types of El Nino and La Nina on summer rainfall over southeast China. J Clim 26:4567–4582

Kim DW, Choi KS, Byun HR (2012) Effecfs of El Nino Modoki on winter precipitation in Korea. Clim Dyn 38:1313–1324

Kug JS, Jin FF, An SI (2009) Two types of El Niño events: cold tongue El Niño and warm pool El Niño. J Clim 22:1499–1515

Larkin NK, Harrison DE (2005) Global seasonal temperature and precipitation anomalies during El Nino autumn and winter. Geophys Res Lett. doi:10.1029/2005GL022860

Li Y, Li J (2012) Propagation of planetary waves in the horizonal non-uniform basic flow. Chin J Geophys 55:361–371 **(in Chinese)**

Li L, Nathan TR (1997) Effects of low-frequency tropical forcing on intraseasonal tropical-extratropical interactions. J Atmos Sci 54:332–346

Li XZ, Zhou W (2012) Quasi-4Yr coupling between El Nino–Southern Oscillation and water vapor transport over East Asia-WNP. J Clim 25:5879–5891

Li SL, Hoerling MP, Peng SL, Weickmann KM (2006) The annular response to tropical Pacific SST forcing. J Clim 19:1802–1819

Li Y, Li J, Jin FF, Zhao S (2015) Interhemispheric propagation of the stationary Rossby waves in a horizontally non-uniform basic flow. J Atmos Sci. doi:10.1175/JAS-D-14-0239.1

Lin H, Derome J (2004) Nonlinearity of the extratropical response to tropical forcing. J Clim 17:2597–2608

López-Parages J, Rodriguez-Fonseca B, Terray L (2015) A mechanism for the multidecadal modulation of ENSO teleconnection with Europe. Clim Dyn 45:867–880

Rayner N et al (2003) Global analyses of sea surface temperature, sea ice, and night marine air temperature since the late nineteenth century. J Geophys Res. doi:10.1029/2002JD002670

Ren HL, Jin FF (2011) Nino indices for two types of ENSO. Geophys Res Lett. doi:10.1029/2010GL046031

Sardeshmukh PD, Hoskins BJ (1988) The generation of global rotational flow by steady idealized tropical divergence. J Atmos Sci 45:1228–1251

Simmons AJ, Wallace JM, Branstator GW (1983) Barotropic wave propagation and instability, and atmospheric teleconnection patterns. J Atmos Sci 40:1363–1392

Simpkins GR, McGregor S, Taschetto AS (2014) Tropical connections to climatic change in the extratropical southern hemisphere: the role of Atlantic SST trends. J Clim 27:4923–4936

Takaya K, Nakamura H (2001) A formulation of a phase-independent wave-activity flux for stationary and migratory quasigeostrophic eddies on a zonally varying basic flow. J Atmos Sci 58:608–627

Ting M, Sardeshmukh PD (1993) Factors determining the extratropical response to equatorial diabatic heating anomalies. J Atmos Sci 50:907–918

Trenberth KE, Caron JM (2000) The Southern Oscillation revisited: sea level pressures, surface temperatures, and precipitation. J Clim 13:4358–4365

Wang X, Wang C (2014) Different impacts of various El Nino events on the Indian Ocean Dipole. Clim Dyn 42:991–1005

Wang B, Wu R, Fu X (2000) Pacific-east Asian teleconnection: how does ENSO affect East Asian climate? J Clim 13:1517–1536

Wang B, Yang J, Zhou T, Wang B (2008a) Interdecadal changes in the major modes of Asian–Australian monsoon variability: strengthening relationship with ENSO since the Late 1970s*. J Clim 21:1771–1789

Wang L, Chen W, Huang R (2008b) Interdecadal modulation of PDO on the impact of ENSO on the east Asian winter monsoon. Geophys Res Lett 35:L20702. doi:10.1029/2008GL035287

Weng H, Ashok K, Behera SK, Rao SA, Yamagata T (2007) Impacts of recent El Niño Modoki on dry/wet conditions in the Pacific rim during boreal summer. Clim Dyn 29:113–129

Weng H, Behera SK, Yamagata T (2009) Anomalous winter climate conditions in the Pacific rim during recent El Niño Modoki and El Niño events. Clim Dyn 32:663–674

Whitham G (1960) A note on group velocity. J Fluid Mech 9:347–352

Wu AM, Hsieh WW (2004) The nonlinear association between ENSO and the Euro–Atlantic winter sea level pressure. Clim Dyn 23:859–868

Wu R, Hu ZZ, Kirtman BP (2003) Evolution of ENSO-related rainfall anomalies in East Asia. J Clim 16:3742–3758

Yang S, Jiang XW (2014) Prediction of eastern and central Pacific ENSO events and their impacts on East Asian climate by the NCEP climate forecast system. J Clim 27:4451–4472

Yu JY, Kim ST (2011) Relationship between extratropoical sea level pressure variations and the central Pacific and eastern Pacific types of ENSO. J Clim 24:708–720

Yu JY, Kim ST (2013) Identifying the types of major El Nino events since 1870. Int J Clima 33:2105–2112

Yuan Y, Yang S, Zhang Z (2012) Different evolutions of the Philippine Sea anticyclone between the Eastern and Central Pacific El Nino: possible effects of Indian Ocean SST. J Clim 25:7867–7883

Zhang W, Jin FF, Zhao JX, Qi L, Ren HL (2013) The Possible Influence of a Nonconventional El Nino on the Severe Autumn Drought of 2009 in Southwest China. J Clim 26:8392–8405

Zhang T, Perlwitz J, Hoerling MP (2014a) What is responsbile for the strong observed asymmetry in teleconnections between El Nino and La Nina? Geophys Res Lett 41:1019–1025

Zhang W, Wang L, Xiang BQ, Qi L, He JH (2014b) Impacts of two types of La Nina on the NAO during boreal winter. Clim Dyn 44:1351–1366

Zhang RH, Li TR, Wen M, Liu L (2015) Role of intraseasonal oscillation in asymmetric impacts of El Nino and La Nina on the rainfall over southern China in boreal winter. Clim Dyn 45:559–567

Zhao S, Li J, Li Y (2015) Dynamics of an interhemispheric teleconnection across the critical latitude through a southerly duct during boreal winter. J Clim. doi:10.1175/JCLI-D-14-00425.1